JPE 12-6-6

http://dx.doi.org/10.6113/JPE.2012.12.6.895

Fast Switching Direct Torque Control Using a Single DC-link Current Sensor

Wei Wang*, Ming Cheng†, Zheng Wang*, and Bangfu Zhang*

†*School of Electrical Engineering, Southeast University, Nanjing, China

Abstract

This paper presents a fast switching direct torque control (FS-DTC) using only a single DC-link current sensor. In FS-DTC, six new active voltage complex space vectors (CSVs) are synthesized by the conventional active voltage space vectors (SVs). The corresponding sectors are rotated in the anticlockwise direction by 30 degrees. A selection table is defined to select the CSVs. Based on the "Different Phase Mode", the output sequence of the selected CSV is optimized. Accordingly, a reconstruction method is proposed to acquire the phase currents. The core of the FS-DTC is that all of the three phase currents can be reliably reconstructed during every two sampling periods, which is the result of the fast switching between different phases. The errors between the reconstructed and actual currents are strictly limited in one sampling period. The FS-DTC has the advantages of the standard DTC scheme such as simple structure, quick torque response and robustness. As can be seen in the analysis, the FS-DTC can be thought of as an equivalent standard DTC scheme with 86.6% of the maximum speed, 173.2% of the torque ripple, and 115% of the response time of the torque. Based on a dSPACE DS1103 controller, the FS-DTC is implemented in an induction machine drive system. The results verify the effectiveness of the FS-DTC.

Key words: Direct torque control, Induction machines, Low-cost drive, Single current sensor

I. INTRODUCTION

Direct torque control (DTC) was proposed in the mid 1980s [1], [2]. Due to its simple structure, quick torque response and robustness, the DTC has received a lot of attention in the literature [3]-[9] and been used widely in the fields such as electric traction, where a fast torque response is required. Essentially, the DTC accomplishes closed-loop control of the stator flux and the electromagnetic torque without current regulators or rotor position information. It is well known that standard DTC (S-DTC) requires the feedback of the phase currents and the DC-link voltage, together with the states of the inverter switches. Therefore, two current sensors and one voltage sensor are always necessary for S-DTC. Additionally, one extra current sensor is always added in the DC-link for over current protection. However, there are two drawbacks to the use of sensors: sensor faults decreases the overall reliability, and the system cost increases with more sensors. Therefore, many efforts have been made to minimize the number of current sensors for electric drive systems. In [10]-[12], several current-sensorless control methods are presented. Although the cost of the drive systems is reduced significantly without current sensors, their dependence on accurate electric machine models weakens system robustness. Since the DC-link current reflects one of the three phase currents when the inverter is operated with active voltage space vectors (SVs), many control schemes with a single current sensor have been presented [13]-[18]. A typical single current sensor drive system is shown in Fig. 1. However, these schemes are mainly focused on the method of pulse width modulation (PWM), while only a few papers, such as [17], [18], are concerned with S-DTC using a single current sensor. The single DC-link current sensor DTC in [17] first predicts the phase currents by an induction machine (IM) model, and then adjusts the predicted phase currents with the measured DC-link current. However, this scheme requires an accurate IM model and more motor parameters in addition to the stator resistance of the IMs, which degrades reliability. The core concept of the scheme using a single DC-link current sensor in [18] is to select an active voltage SV, which reflects a different phase current randomly when the controller is stuck in one phase current for long time. The scheme works well when the switching frequency of the

Manuscript received Mar. 21, 2012; revised Aug. 17, 2012
Recommended for publication by Associate Editor Dong-Hee Lee.
†Corresponding Author: mcheng@seu.edu.cn
Tel: +86-25-83794152, Fax: +86-25-83791696, Southeast University
*School of Electrical Engineering, Southeast University, China

inverter is high, and the estimated phase current matches the measured one well most of the time. However, significant current disturbances and errors between the estimated and measured current in the peaks of the current waveform exist. Because the accuracy of the phase currents is very important for estimating the stator flux and the electromagnetic torque in the DTC, the error of the phase currents degrades the reliability of the control systems. Additionally, the performances become worse at a low switching frequency.

The purpose of this paper is to propose a single-current-sensor-based direct torque control. Both the theoretical analysis and experimental measurements are given to verify the effectiveness of the proposed method. Although an IM is used for exemplification of the control method in this paper, a similar method can be extended to other machines.

II. BASIC CONCEPTS OF S-DTC

In order to clarify the principle of the proposed DTC scheme, the basic concepts of S-DTC are briefly described as follows.

In S-DTC, the stator current $\bar{i}_s$ and voltage $\bar{u}_s$ vectors are obtained by coordinate transformations from the three-phase stationary coordinate *abc* to the two-axis stationary coordinate $\alpha\beta$ by aligning the α-axis along the phase-A of the stator, as:

$$\bar{i}_s = 2(i_{as} + i_{bs}e^{j2\pi/3} + i_{cs}e^{j4\pi/3})/3 \quad (1)$$

$$\bar{u}_s = 2u_{dc}(s_a + s_b e^{j2\pi/3} + s_c e^{j4\pi/3})/3 \quad (2)$$

where u_{dc} is the measured DC-link voltage, s_a, s_b, and s_c are the states of the upper switches of the inverter (s=1 means the switch is closed and s=0 means the switch is open), i_{as} and i_{bs} are the measured phase-A and phase-B currents, and the phase-C current i_{cs} is determined for the Y-connected stator windings by:

$$i_{cs} = -(i_{as} + i_{bs}) \quad (3)$$

The stator flux vector $\bar{\psi}_s$ is computed by:

$$\bar{\psi}_s = \int (\bar{u}_s - \bar{i}_s R_s)dt \quad (4)$$

where R_s is the stator resistance. The stator flux magnitude ψ_s and the electromagnetic torque T_e can be calculated as follows:

$$\psi_s = \sqrt{\psi_{\alpha s}^2 + \psi_{\beta s}^2} \quad (5)$$

$$T_e = 1.5p_n(\psi_{\alpha s}i_{\beta s} - \psi_{\beta s}i_{\alpha s}) \quad (6)$$

where p_n is pole pairs of the IMs, $\psi_{\alpha s}$ and $\psi_{\beta s}$ are α-axis and β-axis components of the stator flux vector $\bar{\psi}_s$, and $i_{\alpha s}$ and $i_{\beta s}$ are the α-axis and β-axis components of $\bar{i}_s$, respectively.

The flux ε_ψ and torque ε_T control signals are generated by two hysteresis comparators:

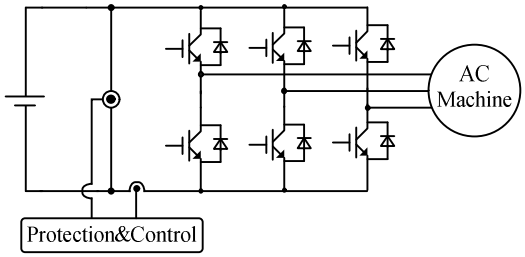

Fig. 1. Configuration of induction machine drive using single DC-link current sensor.

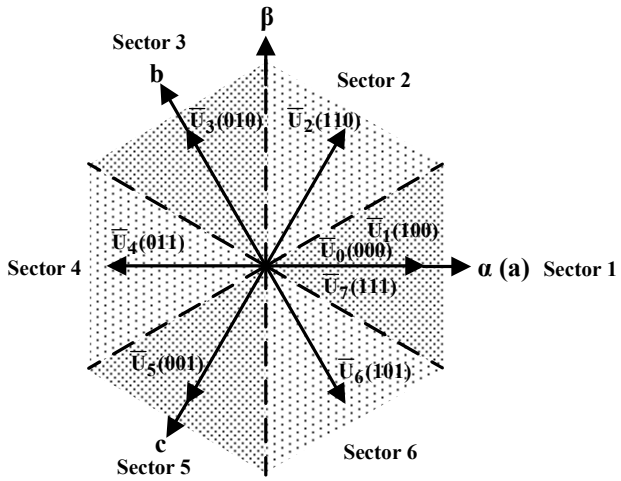

Fig. 2. Distribution diagram of SVs and flux sectors of S-DTC.

$$\varepsilon_\psi = \begin{cases} 1, & if \quad e_\psi > h_\psi/2; \\ 0, & if \quad e_\psi < -h_\psi/2. \end{cases} (e_\psi = \psi_s^* - \psi_s) \quad (7)$$

and:

$$\varepsilon_T = \begin{cases} 1, & if \quad e_T > h_T/2; \\ 0, & if \quad e_T < -h_T/2. \end{cases} (e_T = T_e^* - T_e) \quad (8)$$

where e_ψ and e_T are the errors of stator flux and torque, ψ_s^* and T_e^* are the references of the stator flux magnitude and the electromagnetic torque, and h_ψ and h_T are the hysteresis bands of flux and torque comparators, respectively.

Flux sector N is determined by:

$$\pi(2N-3)/6 <= \theta < \pi(2N-1)/6, N = 1,2,3,4,5,6 \quad (9)$$

where θ is the phase angle of $\bar{\psi}_s$. The distribution of the flux sectors is illustrated in Fig. 2, and the boundaries of the flux sectors are given by the dashed line.

The eight SVs, including the six active SVs ($\bar{U}_1$ - $\bar{U}_6$) and the two zero SVs ($\bar{U}_0$, $\bar{U}_7$), are labeled with the switch states (s_a, s_b, and s_c) and illustrated in Fig. 2. The selection principles of the SVs are listed in TABLE I, in which the zero SVs are not used.

Fig. 3 illustrates a block diagram of the S-DTC.

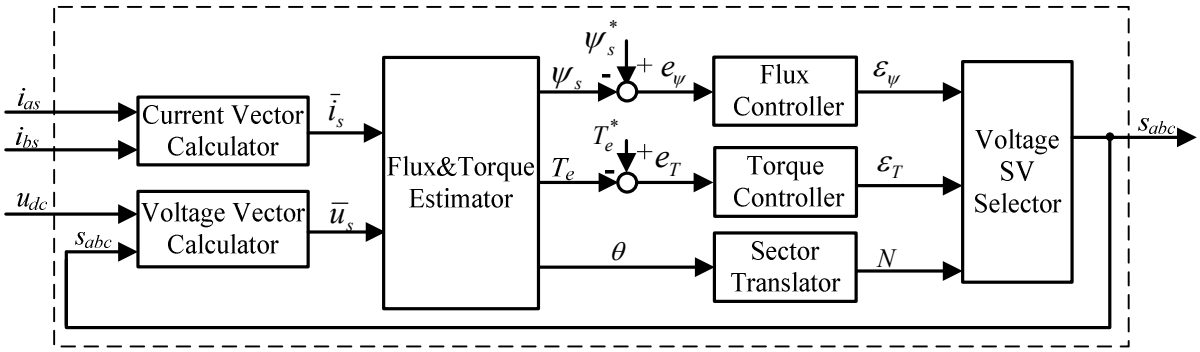

Fig. 3. Control diagram of S-DTC.

TABLE I
SELECTION PRINCIPLES OF SVS OF S-DTC

	ε_T=1		ε_T=0	
	ε_ψ=1	ε_ψ=0	ε_ψ=1	ε_ψ=0
Sector 1	$\overline{U}_2$	$\overline{U}_3$	$\overline{U}_6$	$\overline{U}_5$
Sector 2	$\overline{U}_3$	$\overline{U}_4$	$\overline{U}_1$	$\overline{U}_6$
Sector 3	$\overline{U}_4$	$\overline{U}_5$	$\overline{U}_2$	$\overline{U}_1$
Sector 4	$\overline{U}_5$	$\overline{U}_6$	$\overline{U}_3$	$\overline{U}_2$
Sector 5	$\overline{U}_6$	$\overline{U}_1$	$\overline{U}_4$	$\overline{U}_3$
Sector 6	$\overline{U}_1$	$\overline{U}_2$	$\overline{U}_5$	$\overline{U}_4$

TABLE II
DC-LINK IN-SERIES STATOR PHASE CURRENT VERSUS SVS

$\overline{U}_1$	$\overline{U}_2$	$\overline{U}_3$	$\overline{U}_4$	$\overline{U}_5$	$\overline{U}_6$
$i_{as}=i_{dc}$	$i_{cs}=-i_{dc}$	$i_{bs}=i_{dc}$	$i_{as}=-i_{dc}$	$i_{cs}=i_{dc}$	$i_{bs}=-i_{dc}$

III. PROPOSED DTC SCHEME

When the inverter applies an active SV to the machine, one stator phase is connected in series to the DC-link rail of the inverter, either to the positive or to the negative polarity. Meanwhile, the other two phases are connected in parallel to the opposite polarity. The in-series phase can be easily identified from the states of the upper switches of the inverter, and the current flowing in this phase is either equal or opposite to the DC-link current, as illustrated in TABLE II.

Because only one active SV can be applied in one sampling period, only one phase current can be renewed by a DC-link current sensor in one sampling period. However, two phase currents are needed to execute the DTC scheme, as shown in Fig. 3. In this paper, an improved DTC scheme named fast switching DTC (FS-DTC) is proposed. In the FS-DTC, six new CSVs are synthesized by two adjacent active SVs as shown in Fig. 4:

$$\overline{U}_i = (\overline{U}_j + \overline{U}_k)/2 \tag{10}$$

where $\overline{U}_i$ is a CSV, and $\overline{U}_j$ and $\overline{U}_k$ are two adjacent SVs, (i, j, k)={(I, 1, 2), (II, 2, 3), (III, 3, 4), (IV, 4, 5), (V, 5, 6), (VI, 6, 1)}. According to (10), a CSV can be realized by:

$$\overline{U}_i \times 2T_s = \overline{U}_j \times T_s + \overline{U}_k \times T_s \tag{11}$$

where T_s is the sampling period, $\overline{U}_i$ is a CSV, and $\overline{U}_j$ and $\overline{U}_k$ are two adjacent SVs, (i, j, k)={(I, 1, 2), (II, 2, 3), (III, 3, 4), (IV, 4, 5), (V, 5, 6), (VI, 6, 1)}. If a CSV is selected, one pair of active SVs are selected and these two selected active voltage SVs are executed in turn. Because each SV maintains one sampling period, each CSV maintains two sampling periods. Since adjacent active SVs correspond to different phase currents, two phase currents can be renewed by one CSV in two sampling periods. When compared with the corresponding active SVs, the CSVs are rotated in the anticlockwise direction by 30 degrees, as shown in Fig. 4. To utilize the selection principle of the S-DTC directly, the flux sectors are rotated by 30 degrees accordingly in FS-DTC. The new distribution of the voltage CSVs and the flux sectors is therefore obtained as shown in Fig. 5. The similar selection principle of the CSVs is shown in TABLE III.

TABLE III
SELECTION PRINCIPLES OF CSVS

	ε_T=1		ε_T=0	
	ε_ψ=1	ε_ψ=0	ε_ψ=1	ε_ψ=0
Sector I	$\overline{U}_{II}$	$\overline{U}_{III}$	$\overline{U}_{VI}$	$\overline{U}_V$
Sector II	$\overline{U}_{III}$	$\overline{U}_{IV}$	$\overline{U}_I$	$\overline{U}_{VI}$
Sector III	$\overline{U}_{IV}$	$\overline{U}_V$	$\overline{U}_{II}$	$\overline{U}_I$
Sector IV	$\overline{U}_V$	$\overline{U}_{VI}$	$\overline{U}_{III}$	$\overline{U}_{II}$
Sector V	$\overline{U}_{VI}$	$\overline{U}_I$	$\overline{U}_{IV}$	$\overline{U}_{III}$
Sector VI	$\overline{U}_I$	$\overline{U}_{II}$	$\overline{U}_V$	$\overline{U}_{IV}$

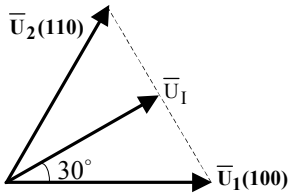

Fig. 4. Synthesis of CSVs (take $\overline{U}_I$ as an example).

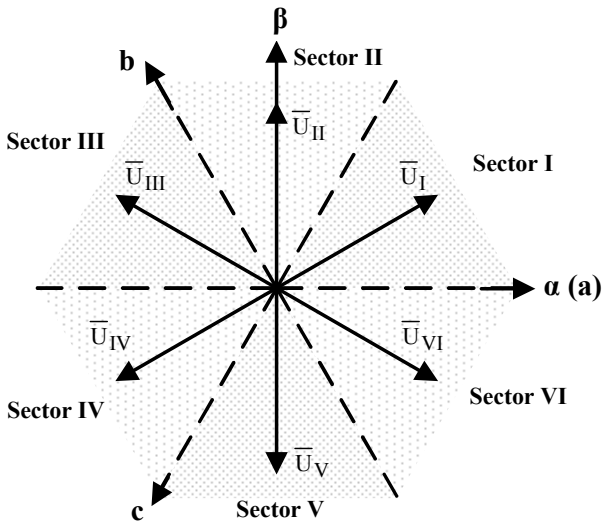

Fig. 5. Distribution diagram of CSVs and flux sectors of FS-DTC.

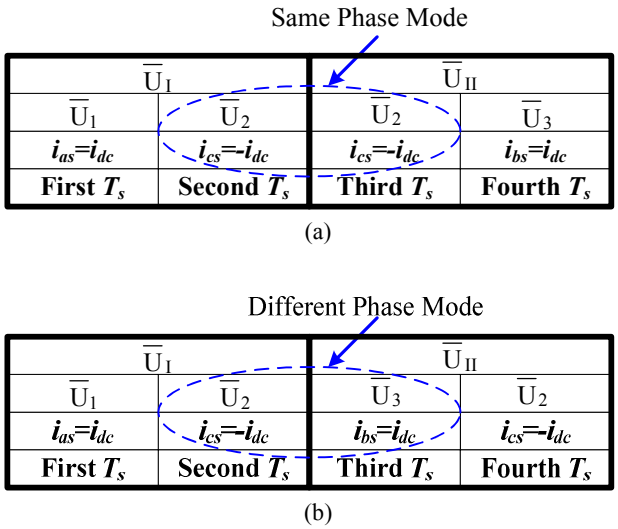

Fig. 6. Output sequences of two voltage SVs included in one CSV. (a) Same Phase Mode; (b) Different Phase Mode.

As mentioned above, one CSV includes two different active SVs. Therefore, there are two different output sequences for each voltage CSV. As an example, Fig. 6 shows two different output sequences for $\overline{U}_I$ and $\overline{U}_{II}$. In Fig. 6(a), the output sequence of $\overline{U}_I$ is $\overline{U}_1 \rightarrow \overline{U}_2$ and the output sequence of $\overline{U}_{II}$ is $\overline{U}_2 \rightarrow \overline{U}_3$. As both of the measured DC-link currents in the second and third sampling periods correspond to the same phase-C current, this output sequence is named the Same Phase Mode. On the other hand, in Fig. 6(b), $\overline{U}_{II}$ is executed by the output sequence of $\overline{U}_3 \rightarrow \overline{U}_2$, and the measured DC-link currents in the second and third sampling periods correspond to two different phase currents. Thus this output sequence is named the Different Phase Mode. To ensure that the two adjacent measured values of the DC-link current correspond to different phase currents, the Different Phase Mode is adopted in this paper.

During every two adjacent sampling periods, the first phase current i_1 is detected in the present sampling period while the second phase current i_2 was detected in previous sampling period, and then the third phase current i_3 is calculated by i_3=-(i_1+i_2). It is clear that both i_2 and i_3 have a delay error of one sampling period. Due to the utilization of the Different Phase Mode, the delay error is strictly limited in one sampling period. Because the phase is changed in every new sampling period, this DTC scheme is named the fast switching DTC.

The FS-DTC is described in Fig. 7. When compared with Fig. 2, the Current Vector Estimator, the New Sector Translator and the Voltage CSV Selector in Fig. 7 replace the Current Vector Calculator, the Sector Translator and the Voltage SV Selector in Fig. 3. In addition, the Optimization Module is added in Fig. 7. The Current Vector Estimator works according to TABLE II. The New Sector Translator determines the flux sectors according to Fig. 5. The Voltage CSV Selector selects the number of CSVs by TABLE III. The Optimization Module optimizes the output sequence of the active SVs for the selected CSVs by the Different Phase Mode.

As is known, induction machines have two important operation modes: traction and regenerative mode. Regardless of the mode, zero vectors are forbidden in the FS-DTC. Therefore, the FS-DTC can be utilized in both traction and regenerative mode.

IV. COMPARATIVE ANALYSIS

In this section, the S-DTC and the FS-DTC are compared. Some simulations are carried out to verify the analysis. To compare the different schemes under equal conditions, a common induction machine is used in all of the simulations, and its parameters are listed in TABLE IV. The other simulation parameters are set as the default values listed in TABLE V if no special declaration is given.

The switching period of the SVs is equal to the sampling period T_s. Because the CSVs are finally realized by the SVs, the actual switching period of the FS-DTC is the same as that of the S-DTC. However, an equivalent switching period is introduced to simplify the analysis since each CSV includes two SVs.

$$T_{sw\_S} = T_{sw\_FS} / 2 = T_s \tag{12}$$

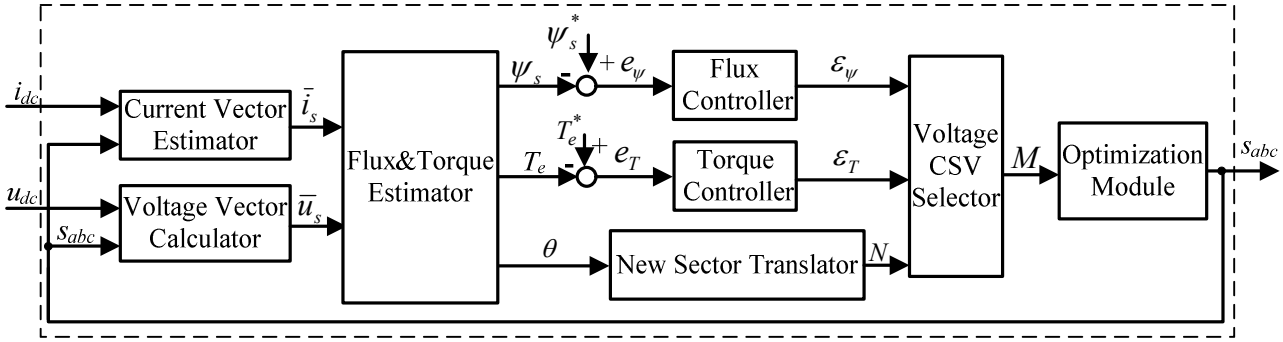

Fig. 7. Control diagram of FS-DTC with single current sensor.

TABLE IV
PARAMETERS OF IM

Parameter	Value
Rated power P_e	5.5 kW
Rated phase voltage V_{rms}	220 V
Rated rotation speed N_n	1450 r/min
Stator resistance R_1	0.628 Ω
Rotor resistance R_2	1.192 Ω
Stator self-inductance L_{11}	5.668 mH
Rotor self-inductance L_{22}	5.668 mH
Mutual inductance L_m	163.9 mH
Pole pairs p_n	2
Inertia J	0.2674 kg·m^2
Friction factor δ	0.0016 N·m·s

TABLE V
DEFAULT VALUES OF SIMULATION AND EXPERIMENTAL PARAMETERS

Experimental parameter	Default value
Sampling period	50 μs
Stator flux reference	0.4 Wb
Load	10 Nm
Speed reference	1000 r/min
DC voltage	200 V

where T_{sw_S} is the actual switching period of the S-DTC and FS-DTC, and T_{sw_FS} is the equivalent switching period of the FS-DTC. Here, T_{sw_FS} is only defined to simplify the analysis and does not actually exist. According to (10), the relation between the amplitude of the SVs and the CSVs is:

$$U_{CSV} = \sqrt{3}U_{SV} / 2 \tag{13}$$

where U_{SV} and U_{CSV} are the amplitude of the SVs and the CSVs, respectively. Therefore, the amplitude of the stator voltage vector can be given by:

$$U_{s\_S} = 2U_{s\_FS} / \sqrt{3} = U_{SV} \tag{14}$$

where U_{s_S} and U_{s_FS} are the amplitudes of the stator voltage vector of S-DTC and FS-DTC, respectively.

According to (12) and (14), there are two differences between the S-DTC and FS-DTC: the switching period (T_{sw_S} and T_{sw_FS}) and the amplitude of the stator voltage vector (U_{s_S} and U_{s_FS}), which result in different performances. In this section, the maximum speed, torque ripple, and response time of the torque are compared.

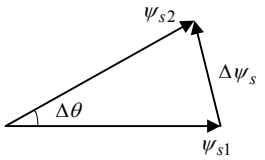

Fig. 8. Response procedure of stator flux of DTC.

TABLE VI
SIMULATION RESULTS OF MAXIMUM ROTATIONAL SPEED

DC voltage (V)	Maximum rotational speed (r/min)		Percentage (%)
	S-DTC	FS-DTC	
150	845	700	82.84
200	1200	1000	83.33
250	1540	1290	83.77
300	1890	1585	83.86
350	2200	1860	84.55

Fig. 8 illustrates the response procedure of the stator flux. In Fig. 8, the amplitude of the stator flux is changed from ψ_{s1} to ψ_{s2} with a flux change of $\Delta\psi_S$. Correspondingly, the phase angle of the stator flux is changed by $\Delta\theta$. To simplify the analysis, both ψ_{s1} and ψ_{s2} are supposed to match the reference ψ_s^* well, that is:

$$\psi_{s1} = \psi_{s2} = \psi_s^* \tag{15}$$

Because it is very small, $\Delta\theta$ can be given by:

$$\Delta\theta \approx \Delta\psi_s / \psi_s^* \tag{16}$$

If the duration of $\Delta\psi_S$ is Δt, the average angular speed $\overline{\omega}$ of the stator flux can be computed by:

$$\overline{\omega} = \Delta\theta / \Delta t \tag{17}$$

According to (14) and the induction machine model, the relationship between the maximum rotational speed under the

S-DTC and FS-DTC can be obtained as:

$$\omega_{FS\_\max} = \sqrt{3}\omega_{S\_\max} / 2 \tag{18}$$

where ω_{S_max} and ω_{FS_max} are the maximum rotor angular speed of the induction machines under the S-DTC and FS-DTC, respectively, and ω_{FS_max} is 86.6% of ω_{S_max}, which is verified by the simulation results listed in TABLE VI.

(6) can be rewritten as:

$$T_e = 1.5 p_n \psi_s i_s \sin\gamma \tag{19}$$

where i_s is the amplitude of $\bar{i}_s$; γ is the angle between $\bar{\psi}_s$ and $\bar{i}_s$. ψ_s and i_s are supposed to be constant during one switching period. The derivation of (19) is:

$$\Delta T_e = k_T \Delta\gamma \tag{20}$$

where k_T=1.5$p_n\psi_s i_s$cosγ, $\Delta\gamma$ is the change of γ in one switching period. Because $\Delta\gamma$ is very small, γ can be supposed to be constant during one switching period. Therefore, k_T is nearly constant during one switching period. It is known that the phase angle of $\bar{i}_s$ can not change suddenly while that of $\bar{\psi}_s$ can. Therefore, $\Delta\gamma$ is nearly equal to $\Delta\theta$ during one switching period. Substituting (12), (17) and (18) into (20) gives:

$$\Delta T_{FS\_\max} = \sqrt{3}\Delta T_{S\_\max} \tag{21}$$

where ΔT_{S_max} and ΔT_{FS_max} are the maximum torque change of the S-DTC and FS-DTC, respectively, during one switching period. It can be seen that ΔT_{FS_max} is 173.2% of ΔT_{S_max}. Because the torque ripple is mainly determined by the maximum torque change in one switching period, the torque ripple of the FS-DTC should be 173.2% that of the S-DTC, which is verified by the simulation results listed in TABLE VII.

Another important performance of DTC is the response time of the torque, which is determined by the change rate of the torque. It is known that ΔT_{S_max} and ΔT_{FS_max} are the torque changes during one switching period while the equivalent switching period of the FS-DTC T_{sw_FS} is different from the switching period of the S-DTC T_{s_FS}. Therefore, according to (12) and (21), the change rate of the torque can be given by:

$$\eta_{FS\_\max} = \sqrt{3}\eta_{S\_\max} / 2 \tag{22}$$

where η_{S_max} and η_{FS_max} are the maximum change rate of torque of the S-DTC and FS-DTC, respectively. It can be seen that η_{FS_max} is 86.6% of η_{S_max}. That is to say, 15.5% of the time will be added to the response of the same torque change for the FS-DTC, which is verified by the simulation shown Fig. 9. In the simulation, the torque is forced to change from -30 Nm to 30 Nm at t=0.001s and the response time of the S-DTC and FS-DTC is 2.6 ms and 3.0 ms, respectively, which matches 15.5% well.

Compared with the S-DTC, the three important performances of the FS-DTC degrade a little, but the ranges of the declines are limited. Generally, FS-DTC can be thought of as an equivalent S-DTC with a half switching frequency deduced from (12) and 86.6% of the DC-link voltage deduced from (14), which will be verified by experiments in Section V.

TABLE VII
SIMULATION RESULTS OF TORQUE RIPPLE

DC voltage (V)	Average torque ripple (Nm) S-DTC	FS-DTC	Percentage (%)
150	0.8	1.3	162.5
200	1.0	1.8	180.0
250	1.4	2.4	171.4
300	1.6	2.7	168.8
350	1.9	3.1	163.1

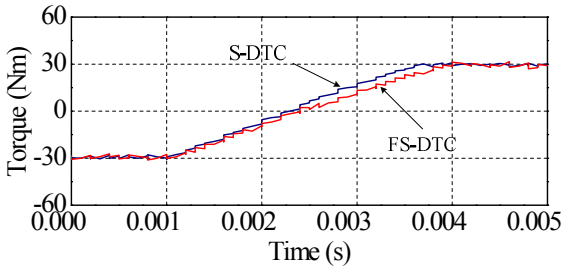

Fig. 9. Comparison of torque response between S-DTC and FS-DTC.

V. EXPERIMENTAL VALIDATION

An experiment platform is developed, as shown in Fig. 10. A DC source supplies the DC-link voltage, and an IGBT-based inverter is used to control a standard 5.5kW IM with an encoder of 1024 pulses per revolution. The parameters of the IM are listed in TABLE IV. The control program is implemented in a dSPACE DS1103 controller. The inputs for the dSPACE DS1103 controller are the measured currents and voltage in the DC-link, and the feedback signal of the encoder. The switch states for the inverter are generated by the dSPACE DS1103 controller. The load for the IM is provided by a permanent magnet synchronous machine (PMSM). A commercial personal computer is employed for editing the control program and commanding the dSPACE DS1103 controller. In this section, the experimental parameters are set as the default values listed in TABLE V if no special declaration is given.

To test the maximum speed, the speed reference is set as 3000r/min which can not be reached by the motor. In the test of the response time of the torque, the torque is forced to change from 10 Nm to -10 Nm.

To check whether the FS-DTC can be thought as an equivalent S-DTC as mentioned in Section IV，a S-DTC scheme with a half switching frequency (10 kHz) and 86.6% of the DC-link voltage (173 V) is also tested in this section, and named H-DTC.

Firstly, the steady-state and transient performances of the FS-DTC are tested and shown in Fig. 11 to 13. As can be seen in Fig. 11(d), Fig. 12(d) and Fig. 13(d), the estimated currents match the measured ones very well in all situations. Due to this important feature, the FS-DTC performed well, which is verified by Fig. 11 to 13. In Fig. 13(b), both the positive torque and the negative torque appear which verifies that the FS-DTC can be utilized in both traction and regenerative modes.

Then, the three DTC schemes (S-DTC, FS-DTC, and H-DTC) are compared in terms of the maximum speed, torque ripple and response time of the torque, respectively, which are illustrated in Fig. 14. As can be seen in Fig. 14, the analysis in Section IV is verified here, that is, the FS-DTC can be thought of as an S-DTC scheme with half switching frequency and 86.6% of the DC-link voltage.

Fig. 10. Diagram of experiment platform.

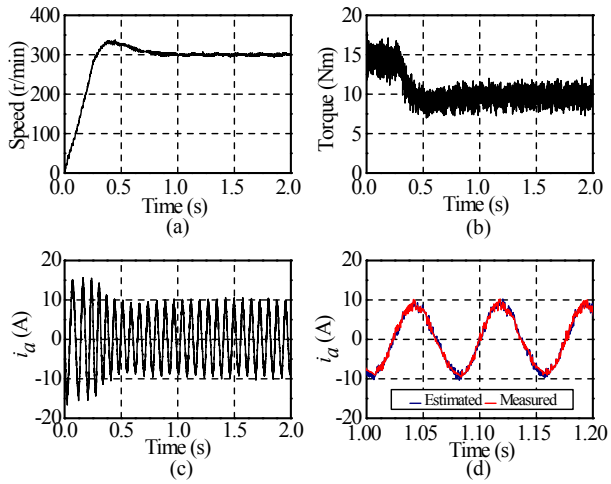

Fig. 11. Steady-state waveforms of FS-DTC @ 300r/min: (a) speed, (b) torque, (c) current of phase-A, (d) portion of (c).

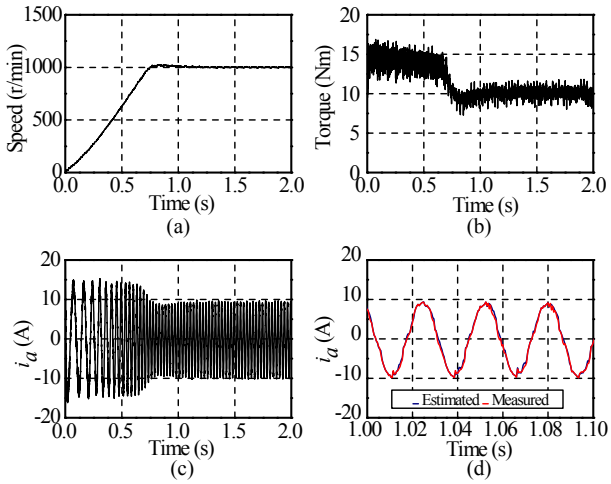

Fig. 12. Steady-state waveforms of FS-DTC @ 1000r/min: (a) speed, (b) torque, (c) current of phase-A, (d) portion of (c).

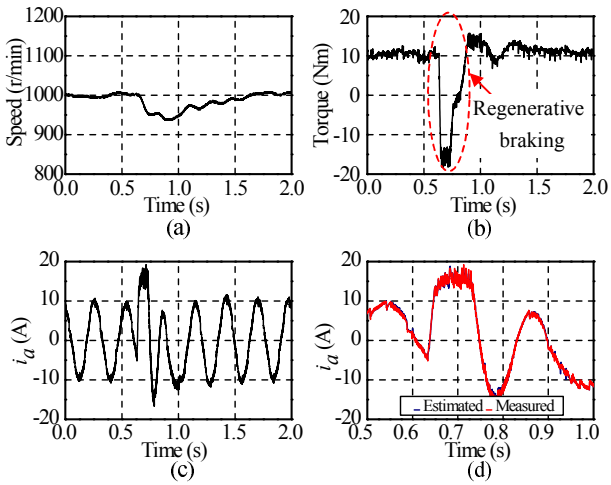

Fig. 13. Transient waveforms of FS-DTC at @ 1000r/min: (a) speed, (b) torque, (c) current of phase-A, (d) portion of (c).

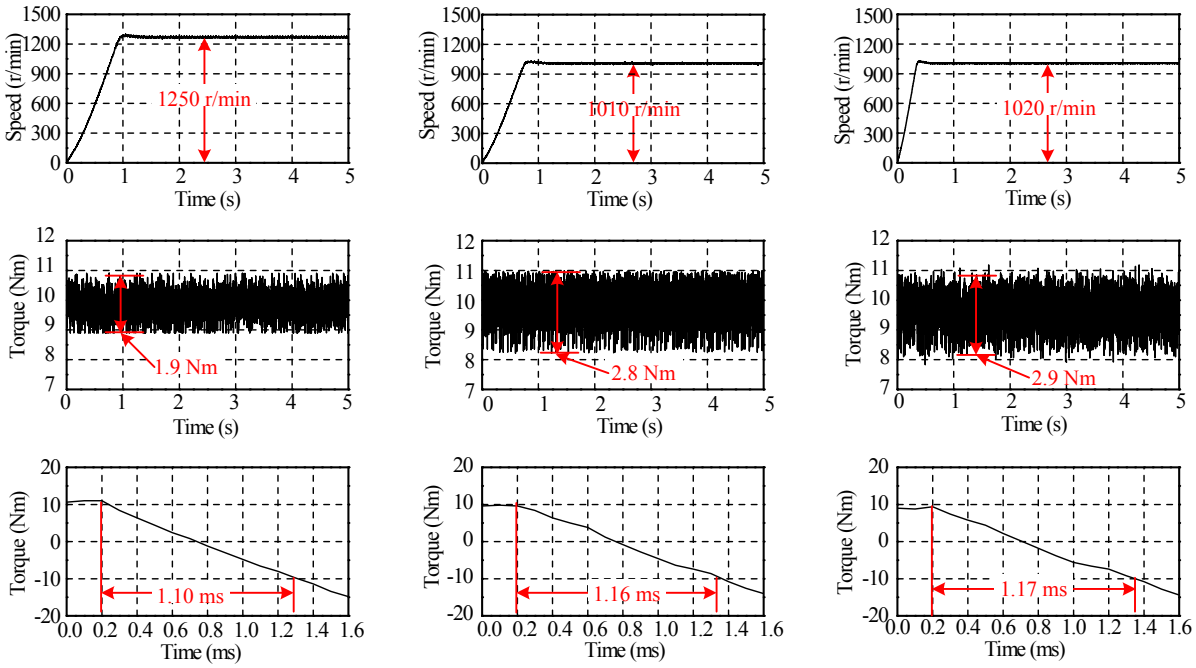

Fig. 14. Comparisons of S-DTC, FS-DTC and H-DTC in the performances of maximum speed (top waveforms), torque ripple (middle waveforms) and response time of torque (bottom waveforms) respectively. (a) S-DTC; (b) FS-DTC; (c) H-DTC.

VI. Conclusions

Due to the pattern of the fast switching between different phases, the FS-DTC can reliably reconstruct the three phase currents by the DC-link current sensor without using more machine parameters. The advantages of a simple structure, the quick torque response and the robustness of the S-DTC are kept by the FS-DTC. When compared with the S-DTC, the FS-DTC has 86.6% of the maximum speed, 173.2% of the torque ripple, and 115% of the response time of the torque. As analyzed in theory and verified by experiments, the FS-DTC can be thought of as an equivalent S-DTC with half switching frequency and 86.6% of the DC-link voltage. Although the performances degrade a little, the FS-DTC operates reliably and performs well in most applications. The FS-DTC can help in the development of low-cost but high-performance drive systems. It can also act as a fault-tolerant strategy to meet phase current sensor faults.

Acknowledgment

This work was supported in part by the National Natural Science Foundation of China (Project 60974060), the Aeronautical Science Foundation of China (Project 20100769004) and a Program Sponsored for Scientific Innovation Research of College Graduates in Jiangsu Province, China (Project: CXZZ_0149).

References

[1] I. Takahashi and T. Noguchi, "A new quick-response and high-efficiency control strategy of an induction motor," *IEEE Trans. Ind. Appl.,* Vol. IA-22, No. 5, pp. 820-827, Sep./Oct. 1986.

[2] M. Depenbrock, "Direct self-control (DSC) of inverter-fed induction machine," *IEEE Trans. Power Electron.,* Vol. 3, No. 4, pp. 420-429, Oct. 1988.

[3] Y. Zhang, J. G. Zhu, W. Xu, and Y. Guo, "A simple method to reduce torque ripple in direct torque controlled permanent magnet synchronous motor by using vectors with variable amplitude and angle," *IEEE Trans. Ind. Electron.,* Vol. 58, No. 7, pp. 2848-2859, Jul. 2011.

[4] W. Wang, M. Cheng, W. Hua, W. Zhao, S. Ding, and Y. Zhu, "An improved stator flux observation strategy for direct torque controlled induction machine drive system," in *Proc. ICEMS*, pp. 863-867, 2010.

[5] W. Wang, M. Cheng, W. Hua, W. Zhao, S. Ding, and Y. Zhu, "Hybrid modeling and applications of virtual metro systems," in *Proc. VPPC*, pp. 1-5, 2010.

[6] A. Ghaderi, T. Umeno, Y. Amano, and S. Masaru, "A novel seamless direct torque control for electric drive vehicles," *Journal of Power Electronics*, Vol. 11, No. 4, pp. 449-455, Jul. 2011.

[7] D. H. Lee, T. H. Kim, and J. W. Ahn, "A hydraulic-oil pump system using sr drive with a direct torque control scheme," *Journal of Power Electronics*, Vol. 9, No. 3, pp. 491-498, May 2009

[8] L. B. Zheng, J. E. Fletcher, B. W. Williams, and X. N. He, "A novel direct torque control scheme for a sensorless five-phase induction motor drive," *IEEE Trans. Ind. Electron.,* Vol. 58, No. 2, pp. 503-513, Feb. 2011.

[9] Y. C. Zhang and J. G. Zhu, "Direct torque control of permanent magnet synchronous motor with reduced torque ripple and commutation frequency," *IEEE Trans. Power Electron.,* Vol. 26, No. 1, pp. 235-248, Jan. 2011.

[10] S. Morimoto, M. Sanada, and Y. Takeda, "High-performance current-sensorless drive for PMSM and SynRM with only low-resolution position sensor," *IEEE Trans. Ind. Appl.,* Vol. 39, No. 3, pp. 792-801, May/Jun. 2003.
[11] A. Consoli, G. Scarcella, and A. Testa, "Speed and current sensorless field oriented induction motor drive operating at low stator frequencies," in *Proc. IAS*, pp. 1679-1686, 2002.
[12] G. Barba, L. Glielmo, V. Perna, and F. Vasca, "Current sensorless induction motor observer and control for hybrid electric vehicles," in *Proc. PESC*, pp. 1224-1229, 2001.
[13] Y. Cho, T. LaBella, and J. Lai, "A three-phase current reconstruction strategy with online current offset compensation using a single current sensor," *IEEE Trans. Ind. Electron.,* Vol. 59, No. 7, pp. 2924-2933, Oct. 2011.
[14] W. Jiang and B. Fahimi, "Current reconstruction techniques for survivable three-phase pwm converters," *IEEE Trans. Power Electron.,* Vol. 25, No. 1, pp. 188 - 192, Jan. 2010.
[15] J. I. Ha, "Current prediction in vector-controlled PWM inverters using single DC-link current sensor," *IEEE Trans. Ind. Electron.,* Vol. 57, No. 2, pp. 716-726, Feb. 2010.
[16] Y. K. Gu, F. L. Ni, D. P Yang, and H. Liu, "Switching state phase shift method for three-phase current reconstruction with a single DC-link current sensor," *IEEE Trans. Ind. Electron.,* Vol. 58, No. 11, pp. 5186-5194, Nov. 2011.
[17] M. Bertoluzzo, G. Buja, and R. Menis, "Direct torque control of an induction motor using a single current sensor," *IEEE Trans. Ind. Electron.,* Vol. 53, No. 3, pp. 778-784, Jun. 2006.
[18] T. G. Habetler and D. M. Divan, "Control strategies for direct torque control using discrete pulse modulation," *IEEE Trans. Ind. Appl.,* Vol. 27, No. 5, pp. 893-901, Sep./Oct. 1991.

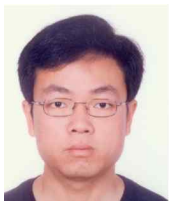

Wei Wang received his B.S. degree in Electrical Engineering from the Nanjing University of Science & Technology, Nanjing, China, in 2008. He is currently working toward his Ph.D. degree in Electrical Engineering at Southeast University, Nanjing, China. From October 2011 to October 2012, he was a joint Ph.D. student with University of Lille 1, Lille, France. His current research interests include electrical machine drives and rail transit.

Ming Cheng received his B.S. and M.S. degrees from the Department of Electrical Engineering, Southeast University, Nanjing, China, in 1982 and 1987, respectively, and his Ph.D. degree from the Department of Electrical and Electronic Engineering, The University of Hong Kong, Hong Kong, in 2001. Since 1987, he has been with Southeast University, where he is currently a Professor in the School of Electrical Engineering and the Director of the Research Center for Wind Power Generation. His current teaching and research interest include electrical machines, motor drives for electric vehicles and renewable energy generation. He has authored or coauthored over 280 technical papers and 5 books, and holds 50 patents in these areas. Prof. Cheng is a Fellow of IET and a Senior Member of IEEE. He has served as a chair and organizing committee member for many international conferences.

Zheng Wang received his B.Eng. and M.Eng. degrees from Southeast University, Nanjing, China, in 2000 and 2003, respectively, and his Ph.D. degree from the University of Hong Kong, Hong Kong, in 2008. From 2008 to 2009, he worked as a Postdoctoral Fellow at Ryerson University, Toronto, Canada. He is currently serving as an Associate Professor at Southeast University. Since 2010, he has been an Honorary Associate Professor of the University of Hong Kong. His current research interests include power electronics and electric drives. He has authored two books and more than twenty international journal papers in these areas.

Bangfu Zhang received his B.S. degree in Electrical Engineering from Huaqiao University, Xiamen, China, in 2010. He is currently working toward his Ph.D. degree in Electrical Engineering at Southeast University, Nanjing, China. His current research interests include electrical machine drives and rail transit.